Indian Journal of Engineering & Materials Sciences
Vol. 31, August 2024, pp. 560-575
DOI: 10.56042/ijems.v31i4.8909

Evaluation of *Ficus krishnae* plant leaves extract as a potent green and sustainable corrosion inhibitor for low-carbon steel in 1.0 M HCl medium

Savitri Danappa Kotabagi[a], Ragini L Minagalavar[a], S K Rajappa[a*], & Ashok M Sajjan[b]

[a]Department of Chemistry, Karnatak Science College, Dharwad, Karnataka 580 001, India

[b]Department of Chemistry, KLE Technological University, Hubballi, Karnataka 580 031, India

Received: 19 February 2024; Accepted: 07 June 2024

Ficus krishnae plant leaf extract (FKLE) has been utilized to mitigate the corrosion of low-carbon steel (LCS) in a 1M HCl environment. The efficacy of *FKLE* on LCS has been evaluated using weight loss measurements, electrochemical impedance spectroscopy (EIS), and potentiodynamic polarization (PDP) techniques. Maximum corrosion inhibition efficiencies of 98.31%, 94.31%, and 96.39% have been observed via weight loss, EIS, and PDP methods respectively, at an optimal concentration of 150 ppm FKLE. The inhibitor molecules have reduced both anodic and cathodic reactions in the acidic medium, demonstrating mixed-type inhibition behavior. Corrosion control has occurred through adsorption phenomena, adhering to the Langmuir adsorption isotherm. Thermodynamic analysis has indicated that the inhibition process is spontaneous and exothermic. Scanning electron microscope (SEM) and transmission electron microscope (TEM) images have revealed severe damage to the LCS surface in the absence of *FKLE*, while significant protection has been provided in its presence. Atomic force microscopy (AFM) images have shown reduced surface roughness on the corroded LCS surface with *FKLE* addition. Water contact angle (WCA) measurements have demonstrated that *FKLE*-treated LCS surfaces possess increased hydrophobicity, whereas untreated LCS surfaces remain more hydrophilic, enhancing susceptibility to acid attack.

Keywords: Low carbon steel, *Ficus krishnae*, Hydrochloric acid, Corrosion inhibition, SEM-EDX

1 Introduction

Corrosion is an electrochemical process that occurs when a metal reacts with its environment, leading to the degradation of materials in various industrial operations. The unexpected loss of metal can be intensified by exposure to acidic environments used in diverse applications such as drilling operations, gas exploration, pickling, acid cleaning processes, and more[1]. Various techniques have been developed to mitigate metal erosion, including lining processes, coatings, the use of corrosion inhibitors, and cathodic protection [2]. Among these methods, the utilization of corrosion inhibitors is particularly significant and commonly employed to reduce the undesirable rate of metal dissolution. Corrosion inhibitors are generally classified into two groups: synthetic-based inhibitors, such as organic inhibitors, and metal-based inhibitors, such as inorganic inhibitors. Previous research has demonstrated that synthetic inhibitors containing heteroatoms, particularly N, O, P, and S, as well as pi bonds and aromatic rings, serve as effective corrosion inhibitors, preventing the oxidative degradation of metals[3]. Epoxy resins are excellent corrosion inhibitors for protecting metallic structures in sulfuric acid solutions[4]. However, due to the hazardous nature of organic inhibitors and their unfavourable environmental impact, natural inhibitor sources have emerged as alternatives. These eco-friendly inhibitors, which include plant extracts, have demonstrated effective metal-inhibiting properties. Moreover, these natural inhibitors are biodegradable, non-toxic, and renewable, rendering them an appealing choice for corrosion control in various industrial settings. Moreover, natural inhibitors tend to be more cost-effective than synthetic alternatives because of their widespread availability and relatively low processing costs. Plant components typically contain bioactive substances with potent antioxidant properties[5-7].

Numerous studies on environmentally friendly green corrosion inhibitors have demonstrated their effectiveness. Previous research suggests that phenolic-rich plant components, terpenes, flavonoids, and various specialized metabolites are equally

*Corresponding author (E-mail: drrajappask@gmail.com)

effective in mitigating and inhibiting the corrosion process, acting similarly to traditional corrosion inhibitors[8]. Earlier studies have demonstrated that components found in plant extracts, including terpenes, phenols, flavonoids, alkaloids, and other active constituents, can interact with metal substrates through various processes. These interactions can involve Coulombic forces, π-electron bonds, or weak intermolecular forces. Additionally, donor-acceptor interactions occur due to electron transfer mechanisms among the heteroatoms of the plant extracts, arenes, or polar functional groups, and the empty d-orbitals of the metal [9]. Moreover, significant research has been undertaken on environmentally friendly corrosion inhibitors, such as the inhibitory effect of *Elettaria cardamomum* pod extract on mild steel corrosion, which demonstrated a 60.6% inhibition rate at a concentration of 250 ppm [10]. In another investigation, Dehghani assessed the inhibitory effects of *Rosemary* extract on mild steel corrosion in a 1M HCl environment. Their findings indicated that at an 800 ppm concentration, this conventional inhibitor mitigated *LCS* corrosion by 92% [11]. Furthermore, D. Prasad found that an extract of *Mimosa pudica* effectively protected mild steel from corrosion in a 0.5 mL/L^- solution, achieving 92% efficiency at a concentration of 500 ppm [12]. Furthermore, it was found by FZ Eddahhaoui that an extract derived from the fruit waste of *Chamaerops humilis* provided a 93% protection efficiency against corrosion of low carbon steel in a 1M HCl solution when used at a concentration of 500ppm [13]. Additionally, A. Thoume found that an extract derived from *Persea americana* leaves exhibited inhibitory properties in a 1M HCl solution. Subsequent polarization investigations revealed a 92% degree of protection in the presence of the hydrochloric acid medium [14].

Numerous studies have been undertaken to mitigate *LCS* corrosion in acidic environments using various plant extracts. Despite these efforts, the currently available products on the market remain insufficient. As a result, this research proposes a bioinspired corrosion inhibitor formulation aimed at enhancing the market appeal of sustainable corrosion inhibitors [8]. The *Ficus krishnae*, commonly known as Krishna Fig and Krishna butter cup, is a species of fig tree belonging to the genus *Ficus* and Moraceae family. It is native to certain regions of India and is characterized by its distinctive large, leathery leaves and spreading canopy. *Ficus krishnae* is also of interest for its potential medicinal properties. *FKLE* leaves has been widely utilized as Ayurvedic medicines to cure the wide range of illnesses, including ulcers, nausea, fever, inflammations, leprosy, syphilis, biliousness, dysentery, and liver inflammation. *FKLE* contains many phytochemicals, these compounds may significantly interact on the metals and alloys surface, hence this property may useful to investigate the corrosion inhibition of various metals and alloys in corrosive environment.

In the present scenario, an attempt was made to utilize the corrosion inhibitive property of the *Ficus krishnae* plant leaf extract for *LCS* in hydrochloric acid medium. Chemical and electrochemical procedures were done to evaluate the inhibitive property, and SEM, TEM, AFM, and water contact angle techniques were adopted to characterize the *LCS* surface morphology change during corrosion.

2 Materials and Methods

2.1 Phytochemical screening

Several tests were conducted to analyze the various phytochemicals constituents of the *FKLE* extract. The Flavonoids Test involved adding magnesium ribbon and concentrated hydrochloric acid to the extract. A change in color to pink, purple, or orange indicated the presence of flavonoids. For the Terpenoids Test, concentrated sulfuric acid and acetic anhydride were mixed with the extract, resulting in a dark red coloration if terpenoids were present. The Tannins Test, known as Braymer's test, utilized ferric chloride solution to detect tannins, indicated by a dirty green precipitate. The Phenolic compounds Test involved mixing the extract with a 5% $FeCl_3$ solution, leading to dark green or bluish-black coloring if phenolic compounds were present. Steroids were identified through a test using chloroform and concentrated sulfuric acid, where the presence of steroids resulted in a visible brown ring. Lastly, the Saponins Test involved mixing the extract with water and observing froth formation after shaking, indicating the presence of saponins. These tests collectively provided insights into the various chemical constituents present in the *FKLE* extract.

2.2 Inhibitor preparation

The plant leaves of *Ficus krishnae* were collected from KLE's Basava Prabhu Kore College in Chikodi,

Belagavi, India**.** After being cleansed with tap water, the fresh leaves shown in Fig. 1(a) were dried under shelter for ten days and then pulverized using a grinder. The powdered sample is shown in Fig. 1(b). The preparation of the extract involved Soxhlet extraction. 25 grams of crushed leaves were extracted for 5 hours in 300 mL of ethanol. To extract the remaining ethanol after extraction, a rotary evaporator was employed.

2.3 Electrolyte preparation

To make the 1.0 M HCl solution, analytical-reagent-grade HCl was diluted with double-distilled water. It served as both a corrosive medium and an electrolyte. For the testing, *FKLE* solutions of differing concentrations produced in a 1.0 M hydrochloric acid solution were used.

2.4 Specimen preparation

After being polished with emery paper of grades 180, 400, 1000, and 2000, *LCS* specimens that were 5 cm long, 1 cm wide, and 0.2 cm thick were cleaned with double-distilled water, dried, and stored in a desiccator. The *LCS* specimens had a percentage composition of: carbon (1.95), aluminium (0.25), silicon (1.19), and iron (96.61). Additional experiments were conducted using the pre-treated materials.

2.5 Weight loss technique

To find the *FKLE* corrosion inhibition in 1.0 M HCl, *LCS* weight-loss research was carried out. Pre-treated coupons were submerged in different *FKLE* concentrations of 1.0 M HCl after being weighed. Coupons were cleaned, dehumidified, and weighed after the test, then placed in a desiccator for storage before being weighed. In the same manner, the average weight loss outcomes were recorded.

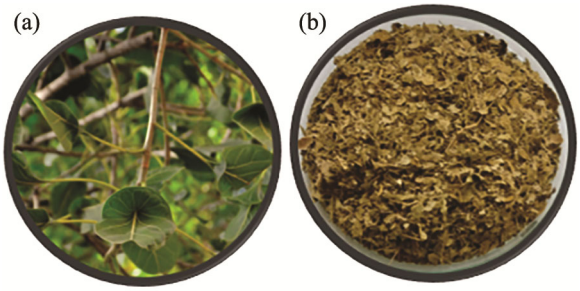

Fig. 1 — *Ficus krishnae* plant leaves a) Fresh leaves, and b) dried leaves powder.

2.6 Electrochemical analysis

Using the CH-Electrochemical equipment type CH1660E, electrochemical techniques such as Potentiodynamic polarization and electrochemical impedance spectroscopy were performed. A three-electrode cell assembly was employed to conduct electrochemical experiments. It consisted of a *LCS* strip of 1 cm^2 exposed area placed in a specimen holder and functioning as the working electrode (WE), a saturated calomel electrode acting as the reference electrode (RE), and a platinum electrode acting as the counter electrode (CE). For forty minutes, to stabilize the open circuit potential (OCP), the *LCS* was submerged in the test solution. With a 200-mV potential range and a 1.0 MV s^{-1} scan rate, the OCP polarization curves were generated. The Nyquist plots were produced in the 0.1 Hz to 100 kHz frequency range, with an amplitude of 5 mV s^{-1}. The required circuit is fitted with Z-simp 3.21 based on Nyquist impedance values.

2.7 Adsorption isotherms and Thermodynamic parameters

The efficacy of *Ficus krishnae* leaf extract in preventing corrosion is dependent on the components adsorbed on the metal surface. For 1.0 M HCl, the adsorption kinetics were evaluated between 300 and 340 ±1K in temperature. Standard techniques are applied, including thermodynamic evaluation of the adsorption kinetics and data fitting into an appropriate model for the adsorption isotherm. The Langmuir adsorption isotherm was coupled to the *FKLE* in this experiment, and several thermodynamic parameters were then computed and presented.

2.8 Fourier-transform infrared spectrum

Using a Nicolet 5700 Fourier-transform infrared spectroscope, the FT-IR spectra of crude *FKLE* and their interaction with the *LCS* surface in 1.0 M HCl were acquired.

2.9 Surface-level investigations

Atomic force microscopy (AFM), scanning electron microscopy (SEM), and transition electron microscopy (TEM) were used to assess the shape of the *LCS* surface. WCA analysis was used to assess the hydrophobicity of the *LCS* surface.

3 Results and discussion

3.1 Screening for phytochemical

The results of the phytochemical investigation for *FKLE* are summarized in Table 1. *Ficus krishnae* leaf extract contains phenolic compounds, flavonoids,

Table 1 — The extract of *Ficus krishnae* leaves contains phytochemicals.

Sl. No.	Constituents of *FKLE*	Name of tests	Results
1.	Flavonoids	Shinoda test	+
2.	Terpenoids	Acetic anhydride + Conc. H_2SO_4 test	+
3.	Tannins	Braymer's test	+
4.	Phenolic compound	5% $FeCl_3$ solution	+
5.	Steroids	Salkowaski's test	+
6.	Saponins	Foam test	+

tannins, steroids, saponins and alkaloids. Most of these substances exhibit significant suppression of corrosion activity[15]. The protective mechanism of Ficus krishnae leaf extract on low carbon steel involves the formation of an adsorption layer. This layer is composed of the various bioactive compounds present in *FKLE*, such as phenolic compounds, flavonoids, tannins, steroids, saponins, and alkaloids. In the presence of the *FKLE* inhibitor, the inhibitor compounds adhere to the metal surface, creating a protective barrier. This adsorption layer effectively shields the *LCS* from further corrosion, enhancing its corrosion resistance in aggressive environments.

3.2 Mass loss measurements

The inhibitory performance of *FKLE* was evaluated using the mass-loss test. The coupons were placed in 100 ml of 1.0 M HCl with varying concentrations of *FKLE* for a duration of one, two, three, four, five, six, and twenty-four hours. Next, each specimen's mass loss at different inhibitor concentrations was compared to the specimen's mass loss in the absence of an inhibitor[16]. For consistency, each experiment was replicated thrice. The mean and standard deviation were calculated. Eqs 1, 2, and 3 were used to calculate the specimen's rate of corrosion, surface coverage (θ), and performance of inhibition (% η_w).

$$\upsilon = \frac{534W}{ATD} \quad \ldots(1)$$

where A stands for the *LCS* area (in square inches), D stands for the *LCS* density, T stands for the submerged duration (in hours), W stands for the weight loss (mg), and υ stands for the low carbon steel corrosion rate (mpy).

$$\theta = \frac{W_1 - W_2}{W_1} \quad \ldots(2)$$

Accordingly, W_1 represents the decrease in mass of *LCS* strips without *FKLE* and W_2 represents the decrease in mass of *LCS* with *FKLE*.

$$\%\eta_W = \frac{W_1 - W_2}{W_1} \times 100 \quad \ldots(3)$$

where W_1 represents the decrease in mass of *LCS* strips without *FKLE* and W_2 represents the decrease in mass of *LCS* with *FKLE*. Table 2 shows the findings of the mass-loss test. The inhibitor's presence in the corrosive medium reduced mass loss over different time intervals, as indicated in the table. Furthermore, an increase in inhibitor concentration enhanced the effectiveness of percentage inhibition. These findings show that *FKLE*'s inhibitory action improves as the concentration of inhibitor in the acid medium rises. The highest inhibitory functionality of *FKLE* at the optimal 150 ppm inhibitor concentration was recorded over a 24-hour immersion time, and it was 98.31%. The interaction between metals and the inhibitor may be weakened by concentrations exceeding 150 ppm of *FKLE*. This weakening can result in the displacement of the inhibitor by H_2O or chloride ions, leading to a reduction in the inhibitor's effectiveness. Acidic solutions also promote the evolution of hydrogen gas. Consequently, no mass accumulates on the surface of the metal. The *FKLE* components undergo protonation in the acidic solution, which slows down the reduction process. Because *FKLE* components stick to the *LCS* surface, which acts as a barrier against corrosive environments, their existence reduces low carbon steel's corrosiveness[17-19].

3.3 Polarization studies

An essential technique for analyzing the kinetics of corrosion, which involves understanding both cathodic and anodic reactions occurring in the corrosion process, is electrochemical polarization measurement. Figure 2 illustrates the Tafel polarization curves for *LCS* specimens immersed in a 1 M HCl solution at a temperature of 300 ± 1 K, both with and without different concentrations of *FKLE*. The electrochemical parameters, including corrosion potential (E_{corr}), corrosion current density (i_{corr}), cathodic (β_c) and anodic (β_a) Tafel slopes, corrosion rate, standard deviation of corrosion rate, and percentage inhibition efficiency (%η_w), are presented in Table 3. The %η_w values were computed using Eq. 4, as provided below [20].

$$\%\eta_w = \frac{i^o_{corr} - i_{corr}}{i^o_{corr}} \times 100 \quad \ldots(4)$$

The electrochemical polarization test assessed the inhibitory effect of *FKLE* on *LCS* in a 1.0 M HCl

Table 2 — LCS mass loss data at 300±1K in 1.0 M HCl at various *FKLE* inhibitor doses.

Time (hours)	Conc. (ppm)	Corrosion rate (mpy)			Mean	Standard Deviation	($\%\eta_W$)	(θ)
		Trial 1	Trial 2	Trial 3				
	Blank	81.99	81.99	78.95	80.98	1.755145		
1	90	15.18	12.15	15.18	14.17	1.749371	81.48	0.8148
	110	9.11	12.15	9.11	10.12	1.755145	88.88	0.8888
	130	6.07	9.11	6.07	7.08	1.755145	92.59	0.9259
	150	3.04	3.04	3.04	6.07	1.749371	96.29	0.9629
	Blank	145.77	148.81	142.73	145.77	3.04		
2	90	18.22	18.22	15.18	17.21	1.755145	87.48	0.8748
	110	15.18	18.22	15.18	16.19	1.755145	89.58	0.8958
	130	12.15	12.15	12.15	12.15	0	91.66	0.9166
	150	9.11	9.11	6.07	8.10	1.755145	93.75	0.9375
	Blank	218.65	221.69	215.62	218.65	3.035001		
3	90	45.55	48.89	48.59	47.68	1.847846	79.16	0.7916
	110	36.44	36.44	33.40	35.43	1.755145	83.33	0.8333
	130	27.33	24.29	27.29	26.30	1.743713	87.50	0.875
	150	12.15	9.11	12.15	11.14	1.755145	94.44	0.9444
	Blank	197.39	200.43	197.43	198.42	1.743713		
4	90	27.33	27.33	27.33	27.33	0	86.15	0.8615
	110	18.22	21.26	18.22	19.23	1.755145	90.76	0.9076
	130	15.18	18.22	15.18	16.19	1.755145	92.30	0.9230
	150	12.14	9.11	9.11	10.12	1.749371	93.84	0.9384
	Blank	212.58	215.62	212.62	213.61	1.743713		
5	90	21.26	24.29	24.29	23.28	1.749371	90.00	0.9000
	110	18.22	18.22	21.26	19.23	1.755145	91.42	0.9142
	130	15.18	12.15	15.18	14.17	1.749371	92.85	0.9285
	150	9.11	12.15	9.11	10.12	1.755145	95.71	0.9571
	Blank	400.86	403.90	403.90	402.89	1.755145		
6	90	45.55	45.55	48.59	46.56	1.755145	88.63	0.8863
	110	42.52	45.55	39.48	42.52	3.035001	89.39	0.8939
	130	30.36	33.41	27.33	30.37	3.040005	92.42	0.9242
	150	21.26	21.26	24.29	22.27	1.749371	94.69	0.9469
	Blank	1618	1624	1621	1621	3		
24	90	45.55	48.59	45.55	46.56	1.755145	97.18	0.9718
	110	39.48	42.52	42.52	41.51	1.755145	97.56	0.9756
	130	30.37	27.33	33.41	30.37	3.04	98.12	0.9812
	150	27.33	27.33	24.29	26.32	1.755145	98.31	0.9831

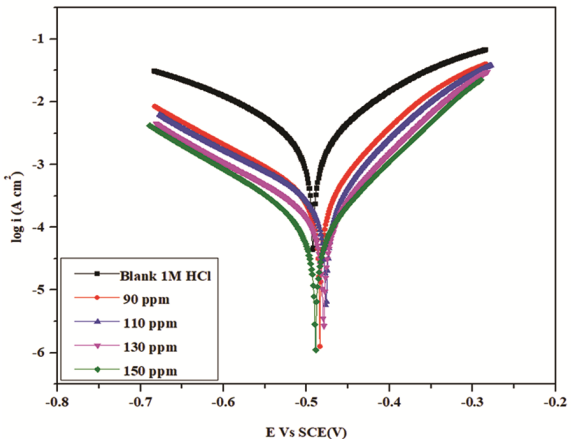

Fig. 2 — Shows the *LCS* polarization curve with and without *FKLE* at various concentrations after it has been dipped in 1.0 M HCl

solution. *LCS* strips were immersed in 1 M HCl containing inhibitor doses of 90, 110, 130, and 150 ppm. The results of the polarization tests are presented in Table 3. Each experiment was conducted three times under identical experimental conditions. For each trial, the corrosion current density and corrosion rate were recorded and are presented in Table 4. Based on the research results, it was observed that the inhibition efficiency of the inhibitor for *LCS* in 1 M HCl medium increased with the addition of concentrations ranging from 90 to 150 ppm. The highest inhibition efficiency of 96.39% was achieved at the highest concentration of 150 ppm. As the inhibitor concentration increased, there was a noticeable decrease in the corrosion current (i_{corr}) without significant impact on the corrosion potential.

Table 3 — The electrochemical polarization approach was used to examine the impact of *FKLE* on *LCS* corrosion in 1.0 M HCl solutions.

Conc. (ppm)	Corrosion Potential (E_{corr}) (V vs SCE)	Corrosion current density (i_{corr}) (A cm^{-2}) Average	Anodic Slope (β_a) (V/dec)	Cathodic Slope ($-\beta_c$) (V/dec)	Corrosion Rate (mil/yr) Average	Standard Deviation	($\%\eta_w$) Average
Blank	-0.48448	$4.39x10^{-3}$	8.007	7.218	$2.03x10^{3}$	0.776416	
90	-0.48326	$5.1x10^{-4}$	12.437	7.187	$2.36x10^{2}$	0.78526	87.46
110	-0.4743	$3.58x10^{-4}$	12.336	6.675	$1.66x10^{2}$	0.282153	91.36
130	-0.48075	$2.55x10^{-4}$	13.179	7.086	$1.18x10^{2}$	0.44679	94.45
150	-0.48903	$1.72x10^{-4}$	12.614	8.620	$0.80x10^{2}$	0.295121	96.10

Table 4 — The electrochemical parameters for each trial.

Corrosion current density (i_{corr}) (A cm^{-2})			Corrosion Rate (mil/yr)			% Inhibition efficiency ($\%\eta_w$)		
Trial 1	Trial 2	Trial 3	Trial 1	Trial 2	Trial 3	Trial 1	Trial 2	Trial 3
$2.794x10^{-3}$	$4.241x10^{-3}$	$6.136x10^{-3}$	$1.292x10^{3}$	$1.96x10^{3}$	$2.84x10^{3}$			
$3.417x10^{-4}$	$5.053x10^{-4}$	$6.827x10^{-4}$	$1.59x10^{2}$	$2.34x10^{2}$	$3.16x10^{2}$	87.77	88.08	86.52
$2.899x10^{-4}$	$3.740x10^{-4}$	$4.114x10^{-4}$	$1.349x10^{2}$	$1.73x10^{2}$	$1.90x10^{2}$	89.62	91.18	93.29
$1.444x10^{-4}$	$2.898x10^{-4}$	$3.295x10^{-4}$	$0.672x10^{2}$	$1.34x10^{2}$	$1.52x10^{2}$	94.83	93.89	94.63
$1.006x10^{-4}$	$1.820x10^{-4}$	$2.329x10^{-4}$	$0.493x10^{2}$	$0.84x10^{2}$	$1.08x10^{2}$	96.39	95.70	96.20

This led to an increase in the inhibition efficiency value [21]. In the presence of inhibitors, the corrosion currents in acidic solutions decrease compared to those without inhibitors. This suggests that increased corrosion inhibition results in a lower proportion of corrosive processes associated with the attachment of inhibitor molecules to the electrode surface[22]. Additionally, the research indicated that the E_{corr} values were higher in the absence of the inhibitor compared to when the inhibitor was present, suggesting that the inhibitor exhibits a mixed mode of action. Furthermore, the anodic and cathodic (βa and βc) slope values show slight changes. This indicates that the inhibitor can effectively mitigate *LCS* corrosion by chemically adsorbing its molecules at both anodic and cathodic sites in the medium, suggesting a mixed mode of inhibition. Table 3 demonstrates the relationship between inhibitor concentration and the decrease in corrosion current density. The results depicted in Fig. 2 reveal a significant pattern: the introduction of an inhibitor results in a distinct movement of polarization curves (both cathodic and anodic) towards lower current densities. This prominent shift indicates successful corrosion mitigation. This is supported by the observed decrease in the corrosion rate of *LCS* when an inhibitor is added to the corrosive environment. The data in Table 3 clarifies that as the concentration of the inhibitor increases, the corrosion rate of the metal decreases in 1.0 M HCl, indicating that *FKLE* shows potential as a powerful inhibitor. With the addition of the inhibitor, the change in corrosion potential (E_{corr}) stays within a range of approximately

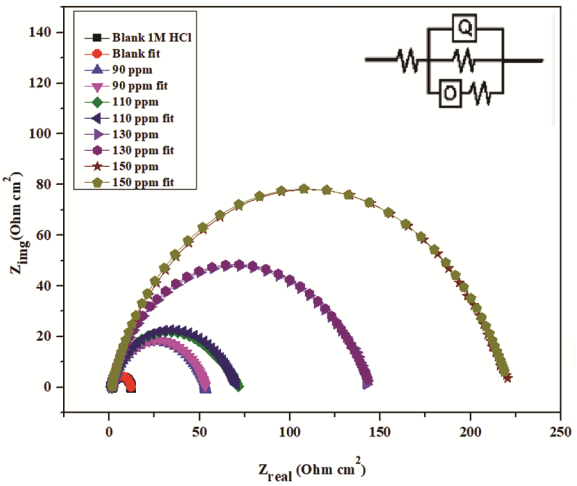

Fig. 3 — Graphs of the Nyquist impedance for *LCS* in 1.0 M hydrochloric acid, in presence and absence of *FKLE* at various concentrations.

-200 mV cathodically and +200 mV anodically, using a scan rate of 1 mVs^{-1} to record the potentiodynamic current-potential curves. This limitation helps to reduce both oxidation at the anode and reduction at the cathode of mild steel[23]. It unveils a dual mechanism that involves both metal dissolution and hydrogen liberation, indicating that *FKLE* effectively controls the corrosion of *LCS* [24].

3.4 Electrochemical impedance spectroscopic determinations (EIS)

With electrochemical impedance spectroscopy, corrosion process monitoring is rapid and easy. Figure 3 displays the impedance Nyquist plots for *LCS* in 1.0 M hydrochloric acid with varying *FKLE*

concentrations and for blank. Surface roughness, inhomogeneity, and inhibitor adsorption changes are correlated with semicircle size. Due to the lower magnitude of the applied voltage, EIS also functions as a harmless assessment. Fig. 3 shows Nyquist plots for *LCS* in the absence and with the change of *FKLE* in a 1.0 M hydrochloric acid solution at 300±1 K. With respect to the charge transfer resistance, the semicircle's diameter will greatly increase. The diameter of the semicircle increased when *FKLE* was added to the acidic media as compared to the blank. As the concentration of *FKLE* increased, it showed more improvement in the semicircle's diameter. This demonstrated how *FKLE* creates a covering layer on its surface and resists the dissolution of *LCS*. It is possible that *FKLE* prevents the corrosion reaction via anodic metal dissolution through a single charge transfer process because Nyquist semicircles in the *FKLE* inhibitor solution show a single capacitive loop that is both inhibited and uninhibited[25]. The degree of agreement between the experimental data from the EIS investigation and a similar circuit model is shown in Fig. 3. At an optimized inhibitor concentration of 150 ppm, the experimental curve generated matches the predicted curve, as shown in Fig. 3. The determined corrosion factors, namely Rs, C_{dl}, and θ, are compiled in Table 5. The computation was done using the Eq. 5 below.

$$\%\eta_w = \frac{R_{ct} - R_{ct,0}}{R_{ct}} \times 100 \quad \ldots (5)$$

There was a maximum $\%\eta_w$of 94.31% as the *FKLE* concentration approached 150 ppm. The width of the semicircle grew. Above this threshold, though, no discernible difference was observed.

The Nyquist charts are connected to the Bode graphs of Fig. 4**,** which exhibit a peak at a middle frequency. In other words, this suggests that the LCS-solution interface's double-charged layer is exclusively connected to a one-time constant. Moreover, Fig. 4 demonstrates how, at lower frequencies, the values of relative impedance increase with *FKLE* concentration. This illustrates the possibility of a significant amount of *FKLE* molecules being adsorbed on the *LCS* surface. More common inhibitor concentrations and more complex charge transport mechanisms are associated with broader adsorption layers[26]. Comparative inhibitory efficacy percentages from various approaches are shown in Fig. 4.

3.5 Temperature effect on Corrosion rate

Mass loss measurements were used to investigate the effect of temperature on the effectiveness of corrosion inhibition on *LCS* surfaces. This was prepared at the optimal inhibitor concentrations, which ranged from 300 to 340 ± K. Table 6 presents the findings. Each experiment was replicated three times under the same experimental conditions. The corrosion rates were calculated for each trial and are summarized in Table 6.

As the temperature rises, the percentage drops, indicating a progressive desorption of the inhibitor molecules from the *LCS* surface. It is found that at higher temperatures, the rate of metal dissolution is faster and the inhibition efficiency is lower. Table 7 shows the results of the different activation parameters for the *LCS* dissolution in acid medium. Elevated E_a^* values indicate that low-carbon steel

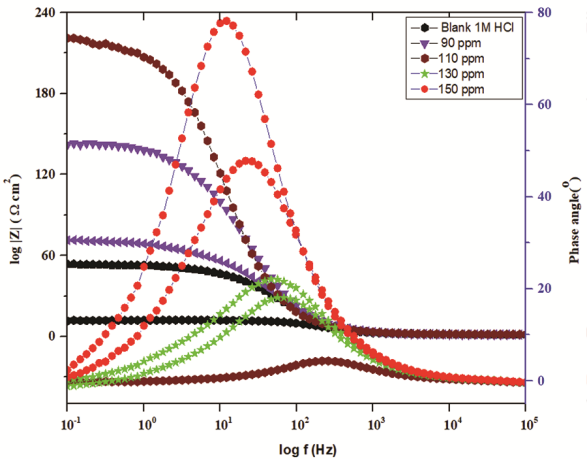

Fig. 4 — Bode graphs for *LCS* at 300±1K in presence and absence of different *FKLE* concentrations.

Table 5 — Results of electrochemical impedance measurement for *LCS* in 1.0 M hydrochloric acid medium at variuos concentration of *FKLE*.

Conc. (ppm)	R_s	Y_o	n	R_{ct} (Ω cm^2)	$C_{dl\ (\mu F\ cm^{-2})}$	L	R_L	$\%\eta_w$
B	1.509	0.000492	0.9845	12.51	0.5926	0.001241	2.136	
90	1.671	0.0002318	1	51.57	0.4532	0.0002153	5.125	75.74
110	1.486	0.0004657	0.9235	71.7	0.3950	0.0005063	724.9	82.55
130	1.468	0.0004589	0.8	152.2	0.3309	0.0003299	139.8	91.78
150	1.659	0.0001994	1	220	0.3275	0.0001576	7.872	94.31

Table 6 — Temperature impact on *LCS* dipped in 1.0 M hydrochloric acid for two hours at different *FKLE* concentrations for 300±1K–340±K

Temp. (K)	Conc. (ppm)	Corrosionrate (mpy)			Mean	Standard Deviation	Percentage inhibition efficiency (%η_w)	Surface coverage (θ)
		Trial 1	Trial 2	Trial 3				
	Blank	145.77	142.73	145.77	144.76	1.76		
300	90	24.29	21.25	27.33	24.29	3.04	87.48	0.8748
	110	15.18	12.15	12.15	13.16	1.75	89.58	0.8958
	130	12.15	15.18	15.18	14.17	1.75	91.66	0.9166
	150	9.11	9.11	6.07	8.10	1.76	93.75	0.9375
	Blank	176.14	179.17	173.10	176.14	3.035		
310	90	36.44	33.405	36.44	35.42	1.76	79.31	0.7931
	110	24.29	27.33	27.33	26.32	1.76	86.21	0.8621
	130	18.22	15.18	18.22	17.21	1.76	89.65	0.8965
	150	15.18	12.15	12.15	13.16	1.75	91.37	0.9137
	Blank	291.54	294.57	288.50	291.54	3.035		
320	90	66.81	63.77	60.73	63.77	3.04	77.08	0.7708
	110	48.59	51.62	48.59	49.6	1.75	83.33	0.8333
	130	33.41	30.37	26.44	30.07	3.49	88.54	0.8854
	150	30.37	33.41	33.41	32.40	1.76	89.58	0.8958
	Blank	695.43	698.48	692.40	695.44	3.04		
330	90	115.40	112.36	118.44	115.4	3.04	83.40	0.8340
	110	109.33	112.36	109.33	110.34	1.75	84.27	0.8427
	130	75.92	78.96	72.88	75.92	3.04	89.08	0.8908
	150	60.73	57.70	57.70	58.71	1.75	91.27	0.9127
	Blank	980.90	977.87	977.87	978.88	1.75		
340	90	227.76	230.80	224.72	227.76	3.04	76.78	0.7678
	110	188.28	191.32	188.28	189.29	1.76	80.80	0.8080
	130	136.66	139.69	133.62	136.66	3.035	86.07	0.8607
	150	121.47	118.43	124.51	121.47	3.04	87.62	0.8762

Table 7 — *LCS* activation parameters in 1.0 M hydrochloric acid both with and without various *FKLE*.

Concentration (ppm)	Activation energy Ea* (kJ mol^{-1}) Trial 1	Trial 2	Trial 3	Average	Standard deviation	Enthalpy of activation ΔH^* (kJ mol^{-1})	Entropy of activation ΔS^* (J mol^{-1} K^{-1})
Blank	100.77	100.17	101.30	100.7467	0.565361	0.20296	-23.713
90	121.13	112.37	110.51	114.67	5.671296	0.30061	-23.702
110	127.45	138.25	125.34	130.3467	6.925318	0.32396	-23.699
130	121.97	141.01	153.06	138.68	15.67542	0.22270	-23.702
150	127.93	134.16	147.43	136.5067	9.95955	0.33488	-23.699

required more energy to dissolve in an acidic medium when an inhibitor was present. When the enthalpy of activation (ΔH^*) is higher in the presence of *FKLE*, it suggests that the process of corrosion of *LCS* is endothermic. Since inhibitor molecules are present on the *LCS* surface, hydrogen ion interaction will be problematic[16]. At the time of degradation, the presence or absence of an inhibitor in a 1.0 M HCl solution does not appreciably change the values of the entropy of activation (ΔS^*).

The Arrhenius Eq. 6 was utilized to investigate the impact of temperature on the rate of corrosion of *LCS*.

$$\text{Slope} = -\frac{\text{Ea}}{2.303\text{R}} \quad \ldots (6)$$

where T stands for the precise temperature, R stands for the universal gas constant, and E_a stands for the activation energy. Figure 5(a**)** displays Arrhenius plots that illustrate the relationship between 1000/T and lnυ_{corr}(mpy). The graphs have a slope of -Ea/2.303R and are straight lines. Figures 5(b) illustrates Arrhenius transition plots, showing the linear relationship between 1000/T and lnυcorr/T (in mpy). These plots exhibit a slope of -Ea/2.303R, indicating a straightforward correlation b) Shows the

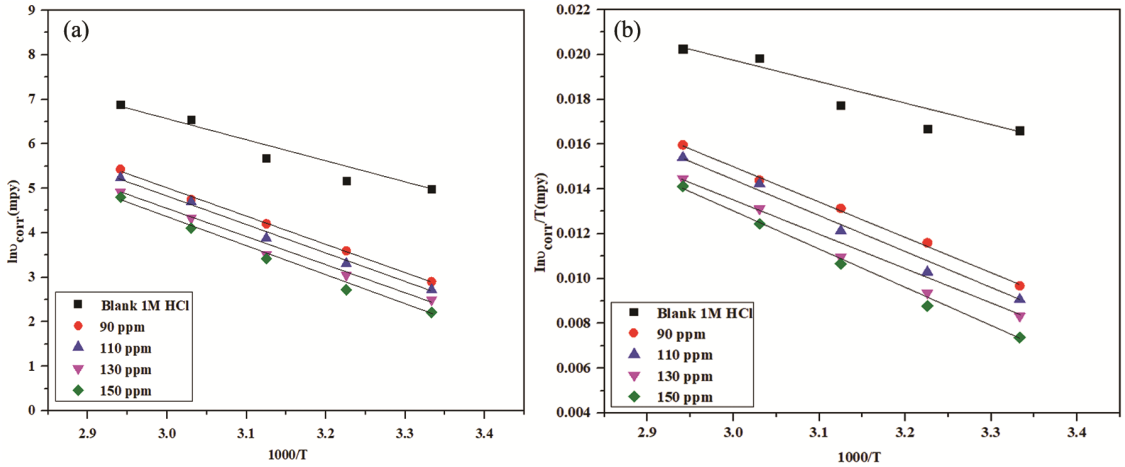

Fig. 5 — a) Arrhenius plots that illustrate the relation between 1000/T and $\ln\upsilon_{corr}$/T(mpy), and b) Transition plots for LCS.

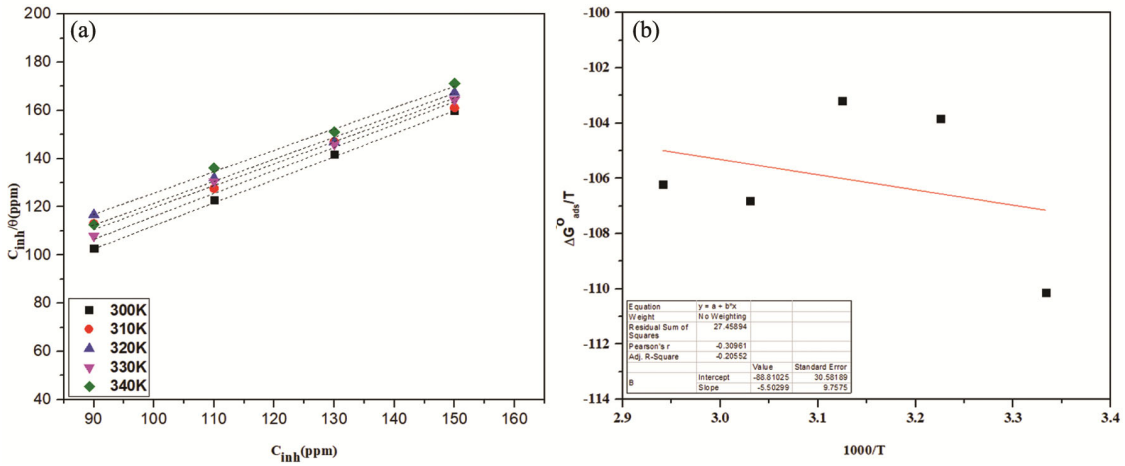

Fig. 6 — a) The graph for the Langmuir adsorption isotherm for varying doses of *FKLE* inhibitor, and b) A graph of ΔG^0_{ads} /T against 1000/T in 1.0 M HCl.

LCS Arrhenius transition graphs in a 1.0 M hydrochloric acid solution with and without *FKLE* inhibitor.

3.6 Adsorption isotherms and thermodynamic parameter computations

Examining *LCS*'s external adsorption process provides crucial information on the corrosion inhibition system. Examining activation energy in depth can result in alterations to the temperature-dependent inhibition efficiency and improvements to the adsorption process[27]. The results showed that mass loss decreased with temperature, which lessened *FKLE*'s inhibitory power. It was found that the activation energy was higher when *FKLE* was present in an acidic media at varying concentrations. This is due to the fact that eliminating the inhibitory compounds from the surface and initiating the metal dissolving process requires more energy due to their larger surface area. *The FKLE* inhibitor could attach itself to the surface of metal chemically, physically, or in a combination of methods, depending on a number of factors, including the solution temperature, the kind of metal, and the electrolyte[28]. The inhibitory effectiveness of the mass reduction technique was utilized to compute the surface coverage. The components of the *FKLE* follow the Langmuir adsorption isotherm, as shown by the plotting of the C_{inh}/θ versus C_{inh} curve (Fig. 6a). Standard Eq. 7 was utilized to assess the adsorption process in this particular model.

$$\frac{C}{\theta} = \frac{1}{K_{ads}} + C \qquad \ldots (7)$$

where θ denotes surface coverage, adsorption equilibrium constant represented by K_{ads}, and C denotes the inhibitor concentration in ppm. By applying Eq. 8, one can ascertain the values of K_{ads} as well as the standard free energy of adsorption G^o_{ads}.

Table 8 — Information on *LCS*'s thermodynamics during *FKLE* adsorption at different temperatures in 1.0 M hydrochloric acid medium.

Temperature (K)	K_{ads} (L mg^{-1})	ΔG^0_{ads} (kJ mol^{-1})	ΔH^0_{ads} (kJ mol^{-1})	ΔS^0_{ads} (J mol^{-1} K^{-1})
300	566.94	-25.836	-6.04146	0.0659
310	256.71	-24.744	-6.04146	0.06033
320	246.10	-25.34	-6.04146	0.060307
330	379.76	-27.32	-6.04146	0.060307
340	353.30	-27.94	-6.04146	0.064407

$$\Delta G^{o}_{ads} = -2.303RT\log\left(K_{ads} \times C_{H_2O}\right) \quad \ldots (8)$$

where the gas constant is R and the temperature is T. and C_{H_2O} is the water concentration in grams per liter. As can be observed in Fig. 6b, the adsorption enthalpy (ΔH^{o}_{ads}) was measured using the slope values of the ΔG^{o}_{ads}/T versus 1000/T plot. The Gibbs Helmholtz Eq. 9 is used to calculate the adsorption entropy (ΔS^{o}_{ads}).

$$\Delta S^{o}_{ads} = \frac{(\Delta H^{o}_{ads} - \Delta G^{o}_{ads})}{T}, \quad \ldots (9)$$

The values of the several thermodynamic parameters, including K_{ads}, ΔG^o, ΔH^o, and ΔS^o, were presented in Table 8. Higher K_{ads} values, according to the results, indicate better *FKLE* inhibitory efficiency as well as increased electrostatic contact between the adsorbed components and the dual layer where two phases converge. The *FKLE* constituents are thermally agitated at a higher temperature, which decreases the whole count of *FKLE* constituents adsorbed on a *LCS* surface and facilitates their interaction with the solution. Physical and chemical adsorption are indicated by ΔG^{o}_{ads} values close to -20 kJ/mol and -40 kJ/mol, respectively. The ΔG^{O}_{ads} values ranged from -25.84 to -27.94 kJ/mol when determined utilizing the standard method for 1.0 M HCl. According to the results, both chemical and physical interactions helped the *FKLE* components adsorb onto the *LCS* surface[29]. The negative statistics demonstrate the exothermic character of the *FKLE* adsorption process, ΔH^{o}_{ads}(-11.40 kJ/mol). Upon the desorption of H_2O molecules, *FKLE* constituents adsorbed on the *LCS* surface, there is a strong indication that the disorder will increase as indicated by positive values of ΔS^{o}_{ads}. This will elevate the adsorption entropy[15].

3.7 FTIR Studies

Numerous phytochemical components, including tannins, flavonoids, terpenoids, steroids, saponins, and phenolic compounds, were detected by the phytochemical screening tests. As can be seen in Figures 7a and 7b, the FT-IR analysis validates these important components, which make up the functional groups. On the specimen's surface, these *FKLE* groups may interact and prevent the corrosion of *LCS*. This example of inhibition was most likely caused by the *FKLE* component adhering to the *LCS* surface and creating a tiny layer of protection on its surface.

Figure 7a represents the Fourier transform infrared spectra for the extracted pure *Ficus krishnae* leaves, show a noticeable -OH band that stretches to a length of 3390 cm^{-1}. The N-H stretching is observable at 2918 cm^{-1}, while at 1707^{-1} cm, the alkene's C=C stretching is apparent. At 1462 cm^{-1}, carboxylic acid's O-H bending can be observed. and 1045cm^{-1} represents strong broad CO-O-CO anhydride stretching frequency. Figure 7b displays the *LCS* meterial's FTIR spectra upon treatment with the chosen inhibitor (*FKLE*) with 1.0 M hydrochloric acid. With respect to pure *Ficus krishnae* leaves extract, these spectra show a significant difference in the functional group's absorbance peaks. The -OH group's extension is demonstrated by the bandwidth at 3434 cm^{-1}. With a frequency of 2924 cm^{-1}, the N-H stretching differs little from the pure *FKLE* extract. The peaks corresponding to C=C stretching of alkene,O-H bending of carbylic acid and anhydride appear at 1630 cm^{-1},1424 cm^{-1} and 1023cm^{-1}. These findings suggest that the *FKLE* extraction contains functional groups, which allow the extract to have a corrosion-inhibiting effect. The pi bond and oxygen (heteroatom) facilitate easy adsorption on *LCS*. Furthermore, because of their strong affinity for electrons, electron-dense substances may rapidly build thin coatings on the surfaces of substrates.

3.8 Scanning electron microscope with EDS analysis

The impact of acid immersion corrosion when *FKLE* is present on the *LCS* surface was evaluated using a scanning electron microscopy method connected to EDX. The morphological features of the adherent coating that developed on the *LCS* strips after they were submerged in the acidic media for 24 hours with the ideal *FKLE* concentration are visible in

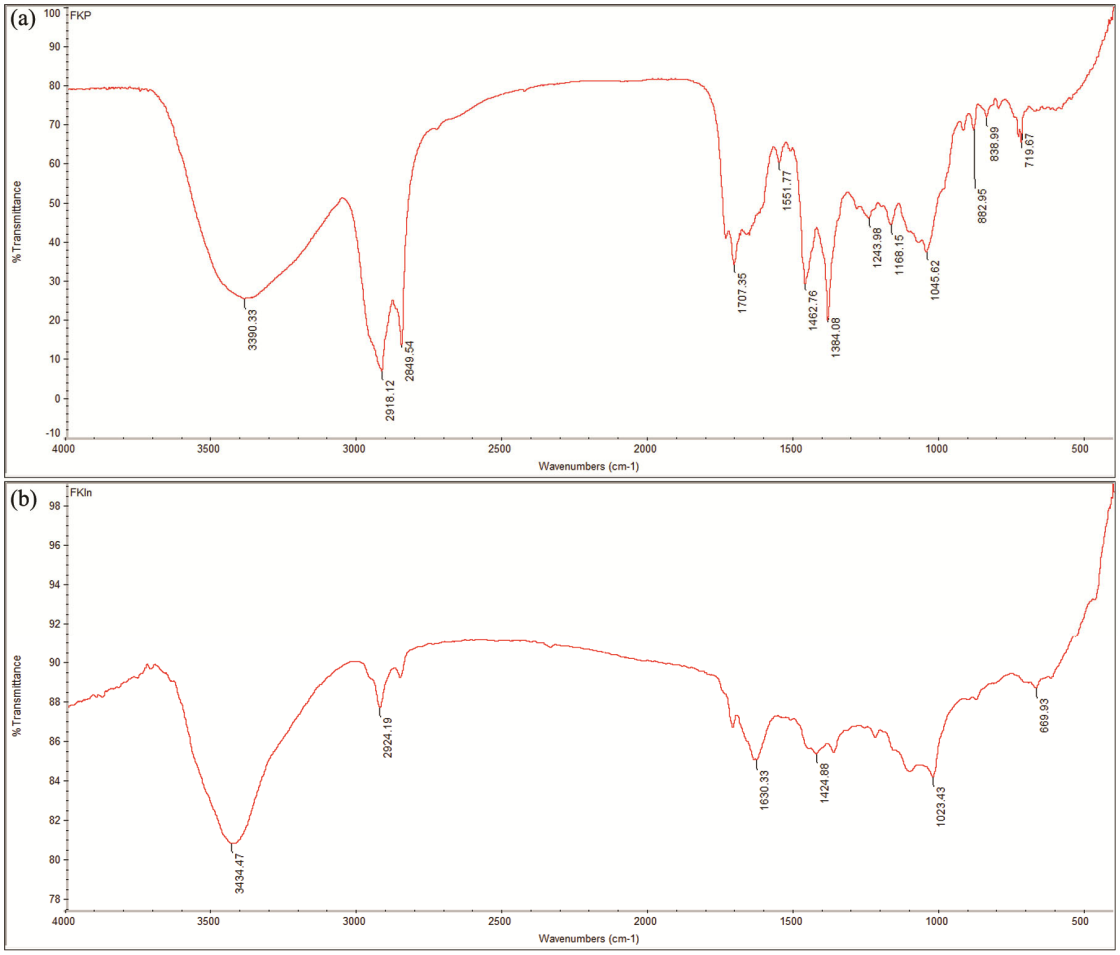

Fig. 7 — a) FTIR spectum of pure *Ficus krishnae* plant leaves extract, and b) FTIR spectrum of scratched *FKLE* compound of immersed electrode surface.

the scanning electron microscopy pictures. Fig. 8a displays a SEM view of a freshly cleaned and polished surface of *LCS*, which is clearly free of scratches. On the other hand, Fig. 8(b) represents the surface of the *LCS* that was dipped in 1.0 M HCl for 24 hours and shows numerous cavities, cracks, and corrosion products because of the acidic assault. Fig. 8c illustrates that the *LCS* was dipped in 1.0 M HCl solutions with 150 ppm of plant inhibitor for 24 hours. The low-carbon steel surface exhibited a smooth surface and was primarily coated with plant molecules, indicating that the plant molecules had adsorbed to the surface and considerably decreased corrosion[30]. Table 9 represents the Fe content of samples (a, b, and c) determined by EDS analysis. Furthermore, it demonstrates how *FKLE* inhibits corrosion by enveloping the test coupon's exterior in a protective coating. The SEM micrographs acquired here validate the results of electrochemical methods and mass reduction[31].

3.9 AFM analysis

Recently, atomic force microscopy has emerged as a new technique for assessing the corrosion inhibitors impact on alloys and metals. This is an effective instrument for determining morphological characteristics at the nano- to microscale. Figure 9(a) represents the 3D AFM images of highly polished, 9b uninhibited, and 9**c** inhibited *FKLE* at optimized concentrations in 1.0 M HCl[32]. The average surface roughness (R_a) of *LCS* obtained from AFM testing is useful in determining the inhibitor's efficacy. The adsorption mechanism of the *FKLE* on *LCS* can be explained by Ra values[33]. Table 10 and Fig. 9 display the average roughness and 3D photos of *LCS* with and without a *FKLE* inhibitor. The depicted abrasiveness findings depict the adsorption mechanism of the inhibitor on *LCS*. Figure 9(a) displays the surface of highly polished *LCS* with a R_a of 153 nm. The *LCS* with a R_a of 1290 nm that was immersed in 1.0 M hydrochloric acid in the absence of an *FKLE* inhibitor

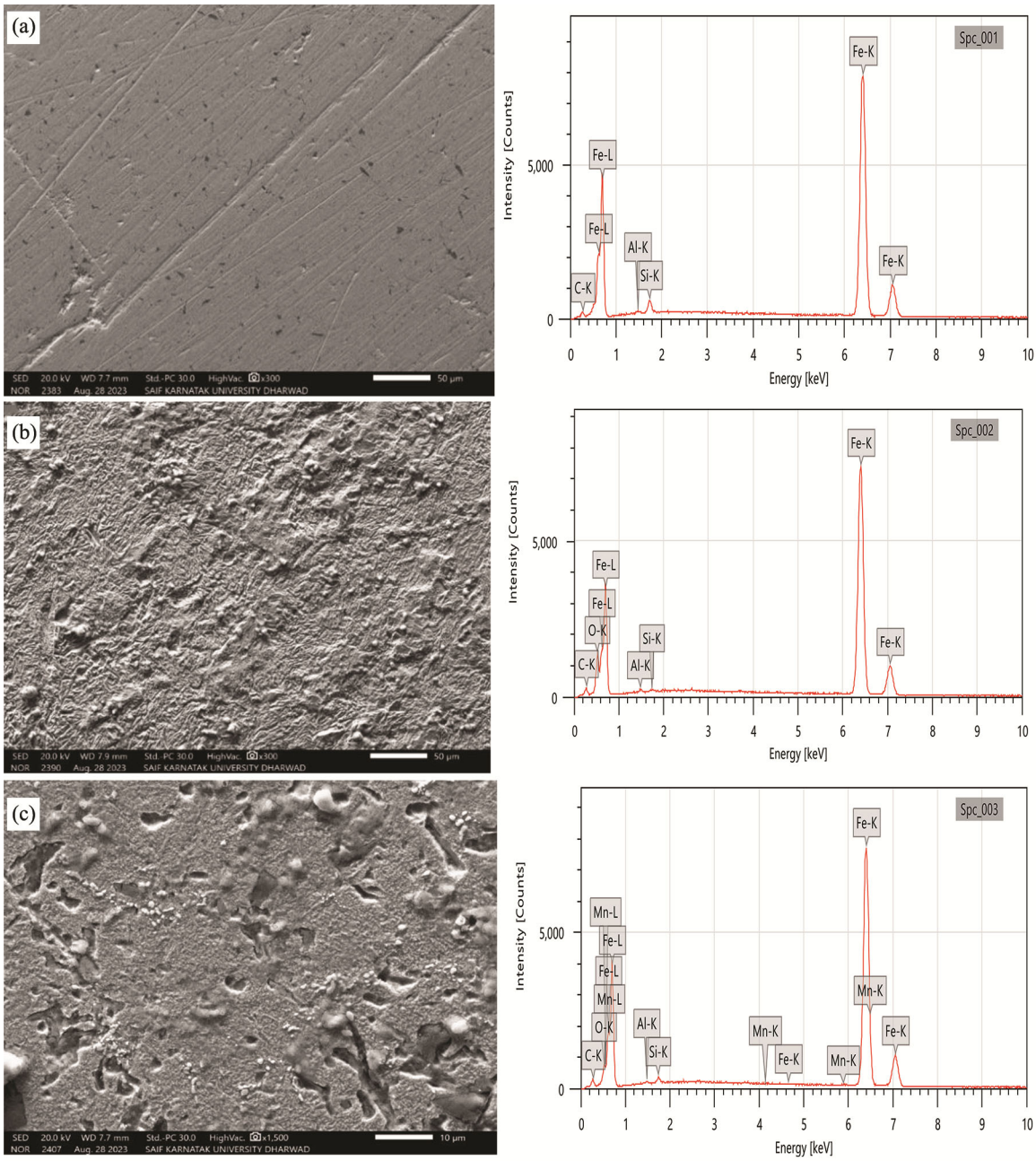

Fig. 8 — Scaning microscopic image of *LCS* a) Highly polished, b) During immersion period of 24 hour in 1.0 M HCl, and c) During immersion period of 24 hour in 1.0 M HCl with 150 ppm of *FKLE*.

Table 9 — Fe content of sample (a, b, and c) determined by EDS analysis.

The percentage composition of Iron		
Sample a	Sample b	Sample c
96.61	90.64	93.44

for 24 hours is displayed in Fig. 9(b). As shown in Fig. 9c**,** the Ra value reported for the *LCS* submerged in 1.0 M HCl with a 150 ppm *FKLE* inhibitor is 986 nm, which is less than the blank one. According to AFM data shown in Table 10, *FKLE* adheres to the *LCS* surface and reduces the rate of corrosion[34].

3.10 Water contact angle tests

A contact angle test was conducted to assess the hydrophobicity and hydrophilicity behavior of the *LCS* surface. As depicted in Fig. 10, the water droplet contact angle was assessed to evaluate the hydrophilicity of the *LCS* surface in the presence and absence of the 150 ppm *FKLE* inhibitor during a 24-

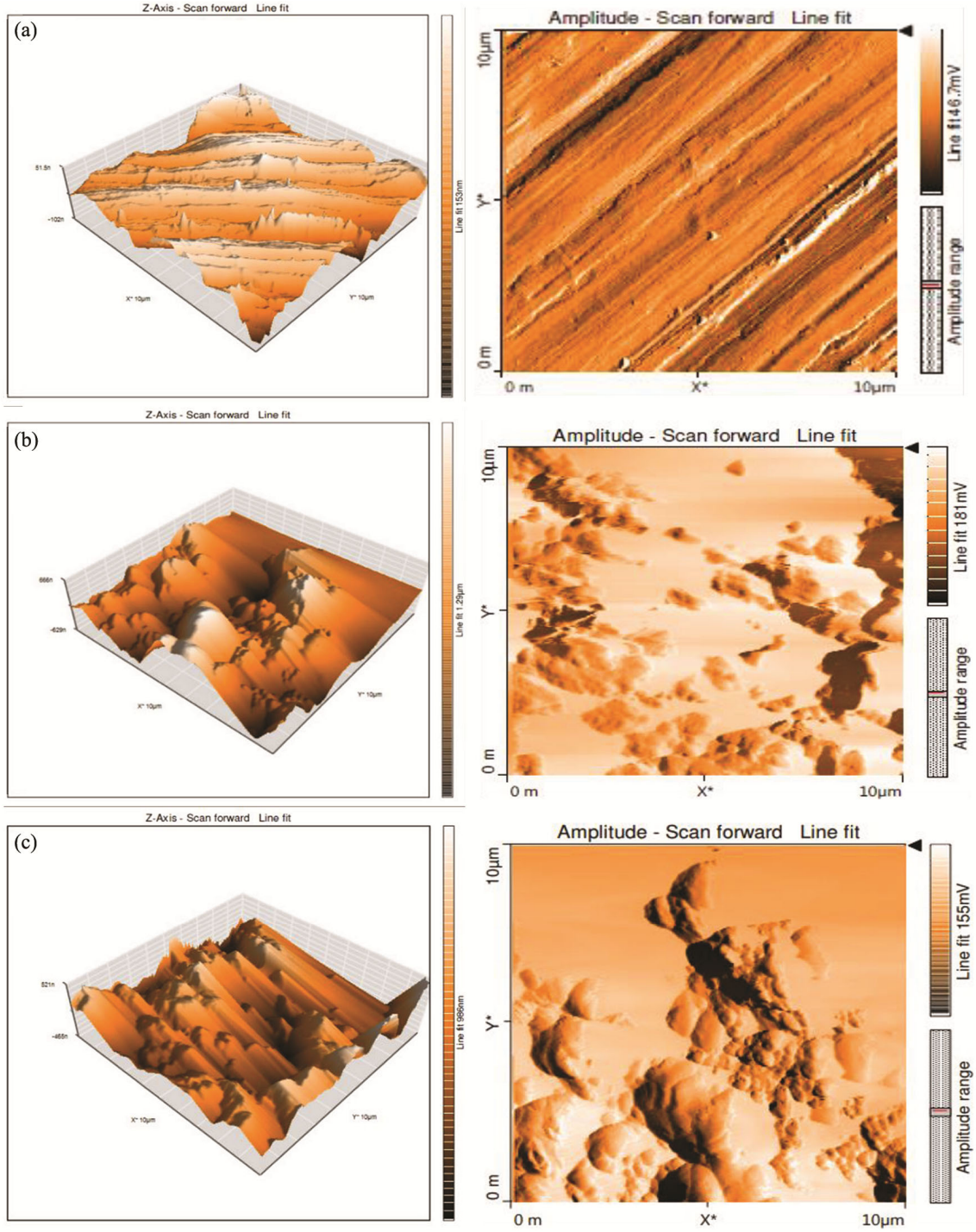

Fig. 9 — 3Dimentional micrographs of AFM a) represents highly polished LCS surface b) LCS dipped for 24 hours in 1.0 M hydrochloric acid, and c) LCS in 1.0 M HCl bearing 150 ppm of *FKLE*.

Table 10 — AFM results of *FKLE*

Specimen	Conc. (ppm)	Average roughness (Ra) (nm)
Polished mild steel	-	153
Blank 1.0 M HCl	-	1290
FKLE	150	986

hour immersion period in 1.0 M HCl. In Fig. 10(a), the water contact angle on the *LCS* surface in 1.0 M HCl without the addition of *FKLE* inhibitor is depicted. The surface exhibits a contact angle value of 32.0°, suggesting a high hydrophilicity nature, which

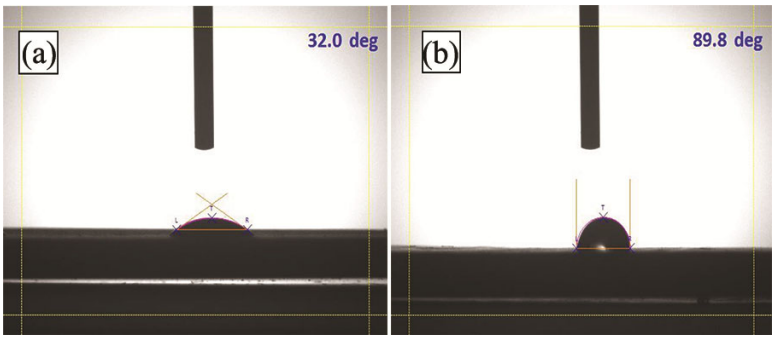

Fig. 10 — WCA images: a) *LCS* dipped in 1.0 M hydrochloric acid (32.0° WCA), and b) *LCS* immersed in 1.0 M hydrochloric acid in addition of 150 ppm of *FKLE* (89.8° WCA).

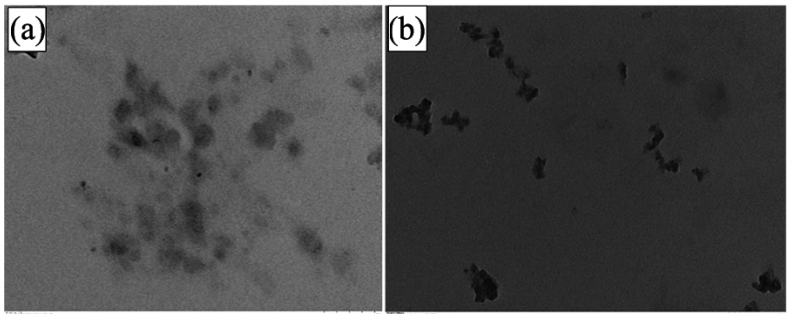

Fig. 11 — Transmission electron microscopy images a) with twenty four hour duration of immersion in 1.0 M HCl, and b) with immersion time of twenty four hour in 1.0 M hydrochloric acid with 150 ppm of *FKLE*.

promotes the metal dissolution process. In Fig. 10b, the water contact angle on the *LCS* surface in 1.0 M HCl with the addition of a 150 ppm *FKLE* inhibitor is illustrated. In the presence of the *FKLE* inhibitor, the *LCS* surface is encapsulated by a thin layer of *FKLE* inhibitor molecules. This layer increases the surface-water contact angle value to 89.8°, indicating a reduced hydrophilicity nature and enhanced hydrophobic nature, which mitigates the metal dissolution process[35].

3.11 TEM analysis

The transmission electron microscopy (TEM) analysis provides detailed insights into the morphological structure of low-carbon steel. This study examines the efficacy of an inhibitor, both with and without its presence, from a morphological perspective *LCS* samples were immersed in a 1.0 M hydrochloric acid solution for a duration of 24 hours, both in the presence and absence of the *FKLE* inhibitor. This experimental setup allowed for a direct comparison of the effects of the inhibitor on the corrosion behavior of the *LCS* surface. Subsequently, the samples underwent a thorough cleaning process involving double-distilled water, followed by drying, to ensure the removal of any residual solution or contaminants. The prepared samples were then subjected to TEM analysis to examine their morphological characteristics and assess the extent of corrosion inhibition provided by the *FKLE* inhibitor. Figure 11(a) presents the surface of *LCS* without the presence of the *FKLE* inhibitor. The surface exhibits notable signs of damage, likely attributed to the corrosive action of the acid solution. This visual evidence underscores the aggressive nature of the acid environment on the *LCS* surface, leading to visible corrosion. In contrast, Fig. 11(b) illustrates the surface of low-carbon steel with the presence of the *FKLE* inhibitor. Here, the surface damage is visibly reduced compared to Fig. 11(a), suggesting that the *FKLE* inhibitor has a protective effect on the *LCS* surface. The presence of the inhibitor appears to mitigate the corrosive impact of the acid solution, leading to a more preserved surface. This observation suggests that the *FKLE* inhibitor has a protective effect on the *LCS* surface, reducing the extent of surface damage caused by the acid solution. This indicates that the presence of the acid solution alone leads to more pronounced metal corrosion, while the combination of the acid solution and *FKLE* inhibitor mitigates this corrosion. The comparison between the two surfaces highlights the protective role of the *FKLE*

Table 11 — Comparing the corrosion inhibition efficiency (%η_w) of *FKLE* with that of other corrosion inhibitors.

Inhibitor type	Name of the corrosion inhibitors	Corrosive medium	Conc.	Maximum %η_w	References	Temp (K)
Synthetic inhibitors	2,20 - {propane-1,3-diylbis [azanylylidene (E) methanylylidene]} bis(6-methoxyphenol)	1 M HCl	0.75mM	95%	36	298K
	(Z)-N-cyclohexyl-1-phenylethan-1-imine	1 M HCl	0.001 M	91%	37	300K
	N-alkylphthalazinone derivative	1M HCl	21×10^{-6}M	93%	38	298K
	1,3,4- oxadiazole	0.5M HCl	50 ppm	84.85%	39	303K
	N, N′-Bis-(2-aminoethyl) piperazine functionalized graphene oxide	15% HCl	25ppm	87%	40	298K
	Quinoxaline-2(1H)-one, derivative	1 M HCl	10^{-3}M	91%	41	328K
	Imidazole-carboxamide derivative	1 M HCl	1×10^{-3} M	90.2%	42	298K
Natural inhibitors	Magnolia grandiflora leaves extract	0.5M H_2SO_4	5.0 g/L	91%	43	303K
	Wood hibiscus leaf extract	0.5M H_2SO_4	160mg/L	92%	44	298K
	Althaea officinalis extract	0.5 M HCl	600 ppm	92.82%	45	298K
	Dillenia suffruticosa leaves extract	1 M HCl	1000ppm	80.4%	46	295.5K.
	Vitex agnus castus leaves extract	1 M HCl	1g/L	81.05%	47	298K
	Artemisia Herba-Alba Leaves	1 M HCl	0.6g/L	93.1%	48	298K
	Eucalyptus (Nilgiris) leaves extract	0.5M HCl	0.5%	95 %	49	303K
	Origanum compactum extract	1 M HCl	400 mgL	90%	50	303 K

inhibitor in reducing the extent of corrosion on the *LCS* surface.

3.12 Comparative study

Numerous researchers have investigated a range of synthetic and natural corrosion inhibitors f or mild steel, with some notable examples listed below, detailing their inhibition efficiency (%η_w) optimized concentration, and operating temperature. *FKLE* stands out with an impressive inhibition efficiency of 98.31%, surpassing the inhibitors listed in Table 11.

4 Conclusions

The present investigation explored the effectiveness of *Ficus krishnae* plant leaf extract as a corrosion inhibitor for low-carbon steel in a 1.0 M hydrochloric acid medium. Chemical and electrochemical analyses revealed a notable decrease in the corrosion rate with increasing inhibitor concentration, reaching a maximum percentage inhibition efficiency of 98.31% at a concentration of 150 ppm. The mechanism of corrosion inhibition was correlated with the adsorption phenomenon, and the adsorption of the inhibitor followed the Langmuir isotherm model. Based on the Tafel curves, ethanolic extract of *Ficus krishnae* plant leaf functioned as a mixed-type inhibitor, tracking the rate of corrosion for both cathodic and anodic reactions. Water contact angle measurements indicated that *FKLE* components render metal surfaces hydrophobic. SEM with an EDS, AFM, and TEM morphological studies revealed a smoother surface of the *LCS* with reduced roughness in the presence of *FKLE*. By creating a shield over the exposed metal surface, *FKLE* shields the *LCS* surface from corrosion. A negative ΔG°_{ads} value indicates that *FKLE* spontaneously adsorbed on the *LCS* surface in the HCl medium.

Acknowledgments

The authors acknowledge the Department of Chemistry at KLE Technological University in Hubballi, India, for providing an electrochemical workstation (CH1660E model), and the DST-SAIF University Scientific and Instruments Centre in Karnatak University Dharwad for providing SEM, AFM and CA spectroscopy capabilities.

References

1 Thoume A I, Nait Irahal N, Benzbiria D, Benmessaoud Left R, Achagar A, Elmakssoudi M, Dakir M, Azzi N, Bourhim & Zertoubi M, *Colloids Surf A: Physicochem Eng,* 674 (2023) 131848.

2 Abbout S, Hsissou R, Erramli H, Chebabe D, Salim R, Kaya S, & Hajjaji N, *J Mol Struct,*1245 (2021) 131014.

3 Abdel-Gaber A, Ezzat A, & Mohamed M, *Sci Rep* 12 (2022) 22251.

4 Dagdag O, Haldhar R, Kim S C, Guo L, Gouri M E, Berdimurodov E, & Ebenso E E, *J Adhes Sci Technol*, *37*(6) (2023) 923.

5 Asadi N, Ramezanzadeh M, Bahlakeh G, & Ramezanzadeh B, *J Taiwan Inst Chem Eng,* 95 (2019) 252.

6 El Ibrahimi B, Baddouh A, Oukhrib R, El Issami S, Hafidi Z, & Bazzi L*, Surf Interfaces* 23 (2021) 100966.

7 Athira R, Poongothai N, Neena P, Babu T S, & Stanley J, *Int J Eng Technol,* 7 (2018) 315.
8 Pai G D, Rathod M R, Rajappa S K, & Kittur A, *Results in Surfaces and Interfaces* 15 (2024) 100203.
9 Chung I M, Malathy R, Priyadharshini R, Hemapriya V, Kim S H, & Prabakaran M*, Mater Today Commun,* 25 (2020) 101687.
10 Shanmugapriya R, Ravi M, Ravi S, Ramasamy M, & Maruthapillai A, *Inorg Chem Commun,* 154 (2023) 110958.
11 Dehghani A, & Ramezanzadeh B, *Ind Crop Prod,* 193 (2023) 116183.
12 Prasad D, Maithani R, & El Ibrahimi B, *J Mol Liq,* 389 (2023) 122940.
13 Eddahhaoui F Z, Najem A, Elhawary M, Boudalia M, Campos O S, Tabyaoui M, Garcia A J, Bellaouchou A, & Amin H M, *J Alloys Compd,* 977 (2024) 173307.
14 Thoume A, Irahal I N, Benzbiria N, Left D B, Achagar R, Elmakssoudi A, Dakir M, Azzi M, & Bourhim, *Colloids Surf A Physicochem Eng Asp, 674* (2023)131848.
15 Rathod M R, Minagalavar R, & Rajappa S K, *J Indian Chem Soc,* 99(5) (2022) 100445.
16 Rathod M R, & Rajappa S K, *Electrochem Sci Adv,* 2(4) (2021) e2100080,
17 Minagalavar R L, Rajappa S K, Rathod M R, & Sajjan A M, *Chem Data Collect, 51* (2024) 101143.
18 Hsissou R, About S, Seghiri R, Rehioui M, Berisha A, Erramli H, Assouag M, & Elharfi A, *J Mater Res Technol,* 9(3) (2020) 2691.
19 Merah S, Larabi L, Benali O, & Harek Y, *Pigment Resin Technol,* 37(5) (2008) 291.
20 Rathod M R, Minagalavar R, & Rajappa S K, *J Ind Chem Soc,* 99 (2022) 100445.
21 Minagalavar R L, Rathod M R, Rajappa S K, & Sajjan A M, *Port Electrochim Acta*, 42 (2024) 233.
22 Zarrok H, Zarrouk A, Hammouti B, Salghi R, Jama C, & Bentiss F, *Corros Sci,* 64 (2012) 243.
23 Minagalavar R L, RATHOD M R, Rajappa S K, & Sajjan A M, *Indian J Chem Techn,* 30 (2023) 492.
24 Rathod M R, Rajappa S K, Praveen B M, & Bharath D, *Curr Res Green Sustain Chem,* 4 (2021) 100113.
25 Al-Fahemi J H, Abdallah M, & EAM Gad, *J Mol Liq,* 222 (2016) 1157.
26 Minagalavar R L, Rajappa S K, Rathod M R, & Sajjan A M, *J Mol Liq* (2023) 123291.
27 Minagalavar R L, Rathod M R, Rajappa S K, & Sajjan A M, *Inorg Chem Commun,* 160 (2024) 111900.
28 Outirite M, Lagrenée M, Lebrini M, Traisnel M, Jama C, Vezin H, & Bentiss F, *Electrochim Acta*, 55(5) (2010) 1670.
29 Kalkhambkar A G, Rajappa S K, & Manjanna J, *Sens Technol*, *2*(1) (2024) 2345081.
30 Kalkhambkar A G, Rajappa S K, Manjanna J, & Malimath G, *Inorg Chem Commun,* 143 (2022) 109799.
31 Guruprasad A, Sachin H, Swetha G, & Prasanna B, *Surf Interfaces,* 19 (2020) 100478.
32 Saxena A, Prasad D, Haldhar R, Singh G, & Kumar A, *J Mol Liq,* 258 (2018) 89.
33 El Azzouzi M, Azzaoui K, Warad I, Hammouti B, Shityakov S, Sabbahi R, & Saoiabi S, *J Mol Liq*, 347 (2022) 118354.
34 Ituen E, Mkpenie V, & Ekemini E, *Physicochem Eng Asp*, 578 (2019) 123597.
35 Sanaei Z, Bahlakeh G, Ramezanzadeh B, & Ramezanzadeh M, *J Mol Liq*, 290 (2019) 111176.
36 Alharthi N H, El Hashemy M A, Derafa W M, Althobaiti I O, & Altaleb H A, *J Saudi Chem Soc,* 26(4) (2022) 101501.
37 Farag A A, Alayyafi A A, Alhussain H, Fawzy A, Masoud E M, & Toghan A, *Inorg Chem Commun,* 163 (2024) 112339.
38 Abdelhadi R A, Ahmed Z E, & Abouzeid A M, *Int J Electrochem Sci,* 18(5) (2023) 100121.
39 Raviprabha K, & Bhat R S, *Egyp J Pet,* 6 (2022) 2311.
40 Haruna K, & Saleh T A, J *Environ Chem Eng,* 9(1) (2021) 104967.
41 Ech-chebab A, Missioui M, Guo L, El Khouja O, Lachhab R, Kharbouch O, Galai M, Ouakki M, Ejbouh A, Dahmani K, & Dkhireche N, *Chem Phys Let,* 809 (2022) 140156.
42 Toghan A, Khairy M, Huang M, & Farag A A, *Int J Electrochem Sci,* 18(3) (2023) 100072.
43 Li B, Wang W, Chen L, Zheng X, Gong M, Fan J, Tang L, Shi Q, & Zhu G, *Int J Electrochem Sci,* 18(4) (2023) 100082.
44 Xu Z, Tan B, Zhang S, Chen J, & Li W, *J Taiwan Inst Chem Eng,* 143 (2023) 104686.
45 Mamudu U, Alnarabiji M S, & Lim R C, *Results in Surfaces and Interfaces*, 13 (2023) 100145.
46 Iranpour M, Babaei A, & Bagherzadeh M, *Results in Surfaces and Interfaces*, 13 (2023) 100163.
47 Hamdouch A, Anejjar A, Bijla L, Gharby S, Asdadi A, Chebli B, Salghi R, & Hassani L I, *Moroc J Chem* 11(1) (2023) 11.
48 Hechiche N, Culioli G, Kadri A, Boughrara D, Saal A, & Perrin F X, *Int J Chem Eng,* 1 (2024) 5432109.
49 Desai P S, Desai F, Patel A, & Parmar B, *Appl Surf Sci Adv,* 16 (2023) 100414.
50 Berrissoul A, Ouarhach A, Benhiba F, Romane A, Guenbour A, Dikici B, Bentiss F, Zarrouk A, & Dafali A, *Ind Crops Prod*, 187 (2022) 115310.